ECS Transactions, 2019, Vol.91, No.1, pp.2399-2408, https://doi.org/10.1149/09101.2399ecst

Perovskite-Like $LaNiO_{3-\delta}$ as Oxygen Electrode Material for Solid Oxide Electrolysis Cells

A.A. Yaremchenko, B.I. Arias-Serrano, K. Zakharchuk, J.R. Frade

CICECO – Aveiro Institute of Materials, Department of Materials and Ceramic Engineering, University of Aveiro, 3810-193 Aveiro, Portugal

Perovskite-like $LaNiO_{3-\delta}$ was evaluated as potential oxygen electrode material for solid oxide electrolysis cells. Compared to the Ruddlesden-Popper $La_{n+1}Ni_nO_{3n+1}$ (n = 1,2,3) counterparts, $LaNiO_{3-\delta}$ exhibits higher *p*-type metallic-like conductivity under oxidizing conditions (450 $S\times cm^{-1}$ at 800°C for highly porous ceramics) together with a moderate thermal expansion coefficient (13.7 $ppm\times K^{-1}$ in air at 25-800°C) compatible with common solid electrolytes. The measured electrode polarization resistance (R_η) in contact with YSZ, CGO and LSGM solid electrolytes was 1.4, 0.77 and 0.22 $\Omega\times cm^2$ at 800°C, and 208, 123 and 7.1 $\Omega\times cm^2$ at 600°C, respectively, under zero-current conditions in air. Surface modification of via PrO_x infiltration resulted in lower values of R_η (0.024 $\Omega\times cm^2$ at 800°C and 0.76 $\Omega\times cm^2$ at 600°C) and low anodic overpotentials (20 mV at 800°C and 500 $mA\times cm^{-2}$) in contact with LSGM.

Introduction

Intermediate-temperature solid oxide cells (IT-SOCs) are emerging as high-efficient electrochemical devices for energy conversion/storage (in solid oxide electrolyser cell operation mode, SOEC) and power generation (in solid oxide fuel cell operation mode, SOFC). Among the most appealing applications of SOECs, the CO_2/H_2O co-electrolysis provides an alternative route to CO_2-capture/recycling and facilitates the integration of the intermittent renewable energy sources into the grid. Nevertheless, the successful implementation of CO_2/H_2O co-electrolysis using SOEC requires to overcome the key barriers mostly related to a poor electrochemical performance of oxygen electrodes. Thus, the development of oxygen electrodes with low polarization losses and the prevention of delamination/degradation at the electrode-electrolyte interface remain the focus of significant research efforts (1,2).

SOECs are essentially based on the same materials and principles as SOFCs. One group of materials particularly promising to act as oxygen electrodes in SOFC devices are K_2NiF_4-type $Ln_2NiO_{4+\delta}$ (Ln =La, Nd, Pr) and its derivatives, due to their high mixed ionic-electronic conductivity, moderate thermal expansion and negligible chemical expansion (3-5). Despite its higher electronic conductivity (6,7), the perovskite-like counterpart $LaNiO_{3-\delta}$ attracted rather negligible attention as an oxygen electrode material apparently because it decomposes at ≈1000°C under ambient oxygen pressure (3,8,9). Furthermore, cathodic polarization may be expected to shift oxygen chemical potential at the electrode towards the low-$p(O_2)$ stability boundary causing its decomposition at the

operation temperature of IT-SOFC. On the contrary, anodic polarization should have an opposite effect thus eliminating the risks associated with the phase stability of $LaNiO_{3-\delta}$ at $T \leq 900°C$.

It is therefore reasonable to consider the utilization of $LaNiO_{3-\delta}$ as a possible oxygen electrode material for SOEC technology. In this work, perovskite-like $LaNiO_{3-\delta}$ was synthesized, characterized by the relevant techniques (XRD, dilatometric and thermogravimetric analysis) and evaluated as a SOEC oxygen electrode employing electrochemical impedance spectroscopy measurements under OCV conditions and under steady-state anodic polarization.

Experimental

Synthesis and ceramic processing

$LaNiO_{3-\delta}$ (LNO) powder was prepared via glycine-nitrate combustion process (GNP) using La_2O_3 (Sigma-Aldrich, ≥99.9%), metallic Ni (Alfa Aesar, 99.9%), HNO_3 and glycine (Sigma-Aldrich, 99%) as fuel agent. Combustion products were fired in air at 800°C for 2 h to remove organic residues, with subsequent calcination steps in oxygen at 800, 900 and 1000°C for 50 h at each temperature. Porous LNO ceramics for electrical and dilatometric studies were sintered in oxygen at 1050°C for 10 h. Solid electrolyte ceramics was prepared using commercial $(ZrO_2)_{0.92}(Y_2O_3)_{0.08}$ (YSZ, Tosoh Corp., ≥99.9%), $Ce_{0.90}Gd_{0.10}O_{1.95-\delta}$ (CGO, Anan Kasei, ≥99.9%) and $La_{0.8}Sr_{0.2}Ga_{0.8}Mg_{0.2}O_{3-\delta}$ (LSGM, Praxair, ≥99.9%) powders. Dense YSZ, CGO and LSGM pellets were sintered in air at 1600°C/10 h, 1600°C/5 h and 1450°C/5 h, respectively.

Materials characterization

X-ray diffraction (XRD, Rigaku D/MAX-B diffractometer, CuK_α radiation) was used to monitor the phase evolution during the synthesis of LNO and to identify possible secondary phases after calcinations of the powdered mixtures of LNO with YSZ, CGO and LSGM. In order to assess the dimensional changes of LNO ceramics during thermal cycling and its thermomechanical compatibility with electrolyte materials, dilatometric experiments (vertical Linseis L75 dilatometer) were conducted in air at 25-950°C with a heating/cooling rate of 3°C/min. Thermogravimetric analysis (TGA) was performed using Setaram SetSys 16/18 instrument (sensitivity 0.4 μg, initial sample weight *ca*. 1.2g) in flowing air to evaluate the oxygen nonstoichiometry (δ) changes. The absolute oxygen content in the reference state (air, 950°C) was determined by TGA *via* in-situ reduction to metallic Ni, coexisting with La_2O_3, in a flowing $10\%H_2$-$90\%N_2$ mixture at 950-1100°C. Electrical conductivity was measured as function of $p(O_2)$ at 700-900 °C using bar-shaped samples by means of standard four-probe DC technique. Pt wires used as current collectors and probes. End-face surfaces of the bar-shaped samples were additionally covered with Pt paint (Heraeus CL11-5349) to improve electrical contact. The flow rate and composition of gas mixtures were set using Bronkhorst mass-flow controllers. Oxygen partial pressure in the gas flow was monitored using an yttria-stabilized zirconia solid-electrolyte sensor.

Electrode fabrication and electrochemical studies

LNO powder (30 vol.%) was added to a solution containing α-terpineol (solvent) and ethyl cellulose (binder, 5 wt.%) and blended using a planetary mill and zirconia balls to produce the electrode ink. In order to prevent the agglomeration of LNO powder, stearic acid (3 wt.%) was added to the ink as a dispersant. Porous LNO layers with an active nominal area of 0.2 cm^2 (5 mm in diameter) were painted onto YSZ, CGO and LSGM solid electrolyte pellets (≈1 mm of thickness) and sintered in oxygen at 1050°C for 2 h. The surface density of consolidated LNO electrode layers was ≈45 $mg \times cm^{-2}$. To enhance the electrocatalytic activity of LNO layers, an aqueous solution of $Pr(NO_3)_3 \bullet 6H_2O$ (Sigma-Aldrich, ≥99.9%; PrO_x load ≈10 wt.%) was infiltrated and fired at 800°C for 2 h to decompose nitrate and obtain uniformly dispersed PrO_x particles on the surface of LNO backbone. The electrochemical activity of LNO and LNO-PrO_x electrode layers was evaluated by electrochemical impedance spectroscopy (EIS) using a AUTOLAB PGSTAT 302 potentiostat/galvanostat (50mV AC amplitude signal, frequency interval 1MHz and 0.01Hz) equipped with a frequency response analyzer (FRA2) module. The measurements were carried out at 800-600°C (50°C step) under zero-current conditions (OCV) using a symmetrical 2-electrode cell configuration and under steady-state anodic polarization employing a 3-electrode cell configuration with Pt counter and reference electrodes. Pt gauzes with Pt wires was used as current collectors. All the tests started by heating the system up to 800°C under flowing air with a heating rate of 3°C/min followed by 15-20 h of stabilization time. Impedance spectra under zero-current conditions were recorded in cooling regime after ≥1 h of stabilization at each temperature. The spectra under anodic polarization conditions were collected in potentiostatic mode with DC potential ranging from 30 to 320 mV (1h stabilization under polarization at each potential step). The electrode microstructural features were assessed by scanning electron microscopy (SEM, Hitachi SU-70 instrument) coupled with an energy-dispersive X-ray spectrometry (EDS, Bruker Quantax 400 detector).

Results and discussion

As-synthesized $LaNiO_{3-\delta}$ (LNO) powder had a rhombohedrally-distorted perovskite-like structure consistent with the *R-3c* ($a^-a^-a^-$) space group (No. 167) and was nearly phase-pure, with negligible peaks of NiO impurity detected in XRD pattern at the background level. LNO ceramic samples sintered in oxygen at 1050°C for 10 h were quite porous and had relative density in the interval 55-58%. The dilatometric results performed in air showed a nearly linear thermal expansion of LNO ceramics (Table I). The corresponding average thermal expansion coefficient (TEC) is given in Table I, together with those obtained for YSZ, CGO and LSGM solid electrolyte ceramics. As shown, porous LNO ceramics exhibits a moderate thermal expansion, with average TEC ≈14 $ppm \times K^{-1}$ at 25-800°C implying a suitable thermomechanical compatibility between the porous LNO electrodes and solid electrolytes in air.

Temperature dependence of oxygen nonstoichiometry (δ) of lanthanum nickelate in air is plotted in Fig.1. Within the stability region in air (T ≤ 1000°C), LNO shows quite low oxygen deficiency. δ is close to 0.010-0.013 oxygen atoms at lower temperatures, and the lattice starts to lose oxygen only on heating above 750°C. The average oxidation state of nickel cations is close to 3+. One should note that small δ values indicate a very

low concentration of oxygen vacancies in the LNO lattice suggesting a limited contribution of oxygen-ionic transport to the total electrical conductivity.

TABLE I. Average thermal expansion coefficients (TECs) in air.

Material	T, °C	TEC, ppm×K^{-1}
LNO	25-950	13.7
YSZ	25-1100	10.7
CGO	25-1100	12.4
LSGM	25-1100	11.0

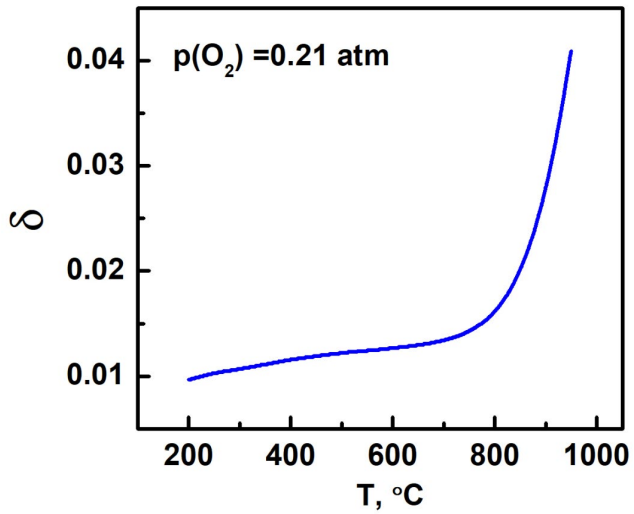

Figure 1. Temperature dependence of oxygen nonstoichiometry of LNO in air.

In agreement with literature data (3,6,7), LNO ceramics showed quite high metallic-like electrical conductivity decreasing with increasing temperature. Fig.2 shows $p(O_2)$-dependences of electrical conductivity at 700-900°C within the stability domain of the perovskite phase. One should stress that even highly porous samples (porosity > 40%) exhibit the conductivity values as high as 450 S×cm^{-1} at 800°C in air. This is 5-10 times higher compared to Ruddlesden-Popper $La_{n+1}Ni_nO_{3n+1}$ (n = 1, 2, 3) counterparts under the same conditions (6).

Electrical conductivity of LNO was found to increase with increasing oxygen partial pressure (Fig.2). This behaviour can be interpreted considering the defect chemistry of lanthanum nickelate. High metallic-like conductivity of this oxide is attributed to the transformation of the partially filled e_g orbitals of Ni^{3+} cations (low-spin $t_{2g}^6 e_g^1$ state) into partially filled σ* conduction band states (7). Increasing $p(O_2)$ under isothermal conditions results in an incorporation of oxygen into the crystal lattice which leads to a lower oxygen vacancy concentration, lower fraction of Ni^{2+} in the B sublattice and larger fraction of Ni^{3+}:

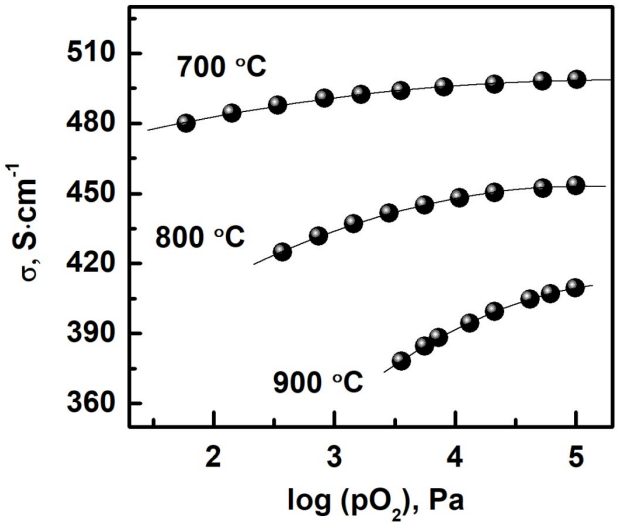

Figure 2. Oxygen partial pressure dependence of total conductivity of porous LNO ceramics at 700-900°C under oxidizing conditions.

$$2Ni^{2+} + V_O + 0.5O_2 \xleftrightarrow{K_{ox}} 2Ni^{3+} + O_O^{2-} \quad [1]$$

Thus, higher oxygen partial pressure results in a higher concentration of itinerant charge carriers (equivalent to $[Ni^{3+}]$), their higher mobility (due to lower scattering on Ni^{2+} cations) and, therefore, higher electronic transport. At the same time, changes in electrical conductivity are rather moderate, especially at higher oxygen pressures corresponding to the anodic polarization conditions, suggesting a stable electrical behavior of the electrode layers during the operation.

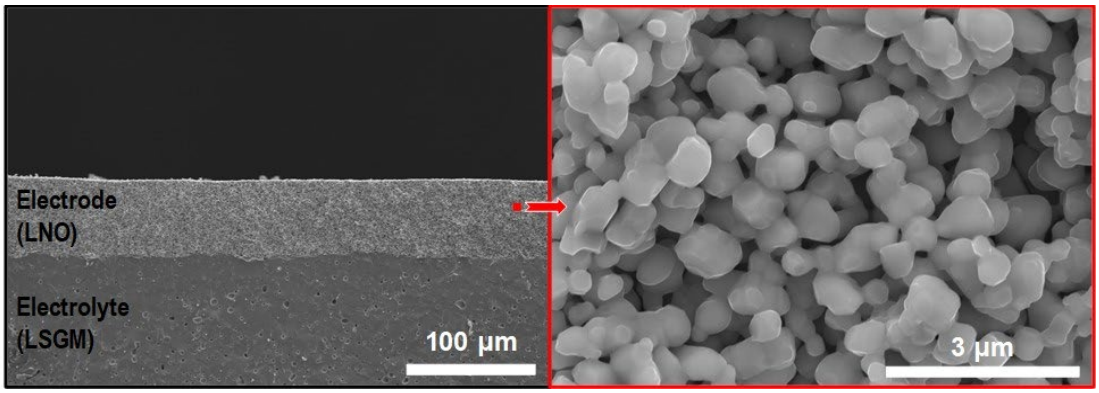

Figure 3. SEM micrographs: (A) cross-sectional view of porous LNO electrode applied onto LSGM electrolyte, and (B) microstructure of LNO electrode.

Fig.3 shows representative micrographs of a fractured cross-section of the electrode/electrolyte assembly - LNO||LSGM in a given particular example. Porous LNO appears to be evenly distributed over the surface of the LSGM. Moreover, no evidence of reactivity products could be found at the electrode/electrolyte interface. Typically, the thickness of the LNO layer was 55-65 µm with the particle size ranging from 0.4 to 1 µm.

Additionally, the porosity network appears to be formed by fine and fully interconnected channels which should favor the gas diffusion through the LNO microstructure.

By means of EIS measurements under zero-current conditions, the electrochemical response of the symmetrical 2-electrode cells may be separated into ohmic resistance the cell and polarization resistance of electrodes. Characteristic spectra collected under zero-current conditions and corresponding to the response of LNO||YSZ, LNO||CGO and LNO||LSGM cells at 800°C are represented in Fig 4A. All spectra were satisfactorily fitted using an equivalent circuit consisting of an inductance (L) element in series with an ohmic resistance (Ro) and two low-frequency (R-CPE) contributions to the Nyquist plot (Fig.4B). The pseudo-capacitances associated with the low frequency contributions ranged from $2 \cdot 10^{-4}$ to $7 \cdot 10^{-3}$ Fcm^{-2} (LF1) and from $2 \cdot 10^{-3}$ to $1 \cdot 10^{-2}$ Fcm^{-2} (LF2). Taking into account these pseudo-capacitance values and the results reported elsewhere (10,11,12), LF1 is expected to be associated with the gas diffusion processes, and LF2 can be ascribed to the activation of the electrocatalytic processes (*e.g.* OER - oxygen evolution reaction).

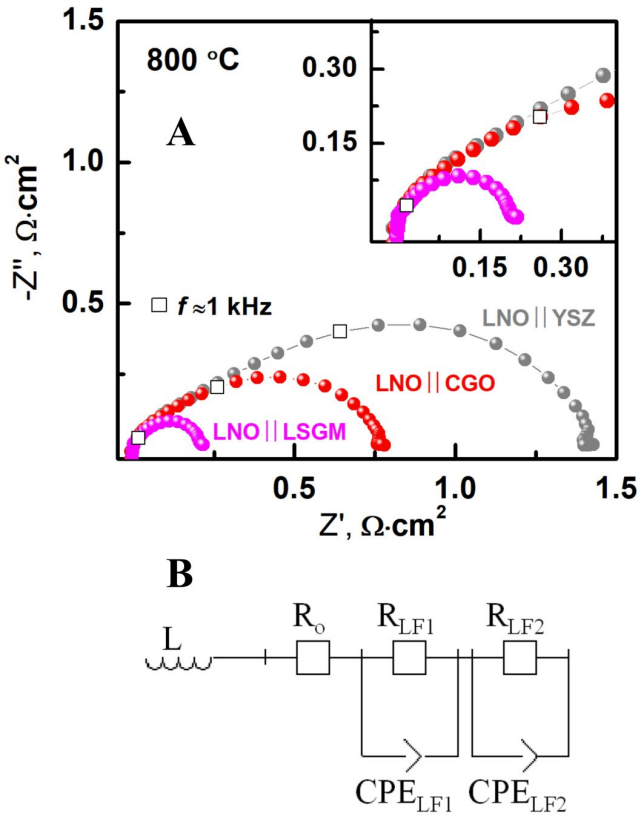

Fig.4. (A) Nyquist plot of LNO electrodes in contact with YSZ, CGO and LSGM electrolytes in air at 800°C under zero-current conditions, and (B) equivalent circuit used to fit the experimental data. Open squares in (A) correspond to frequency of 1kHz.

Table II lists the measured values of polarization resistance (R_η) at 600-800°C and corresponding activation energy (E_A) for different symmetrical cells with 2-electrode configuration. Increasing temperature facilitates the transport processes and favors the activation of the electrochemical reactions and leads to a decrease in polarization

resistance. The cells based on YSZ and CGO solid electrolytes demonstrate significantly worse performance compared to the cells based on LSGM, especially at lower temperatures. At all studied temperatures, the polarization resistance on LNO electrodes in contact with different solid electrolytes decreases in a row YSZ < CGO < LSGM (Table II). This is also accompanied by a change in the activation energy of electrode process which is similar for LNO||YSZ and LNO||CGO electrodes (≈2.1 eV) but decreases down to 1.5 eV for LNO||LSGM cells.

Table II. Polarization resistance (R_η) of LNO-based electrodes in contract with different solid electrolytes and corresponding activation energy in air at 600-800°C.

Electrode ‖ Electrolyte	**R_η, Ω·cm^2**			**E_A, eV**
	800°C	**700°C**	**600°C**	
LNO||YSZ	1.41	17.3	208	2.10
LNO||CGO	0.77	8.99	123	2.13
LNO||LSGM	0.22	1.04	7.14	1.50
LNO + PrO_x||LSGM	0.024	0.11	0.76	1.48

Note: The activation energy E_A is calculated using Arrhenius equation $1/R_p = (A_0/T)\exp(-E_A/(RT))$.

Comparatively worse electrochemical performance of the LNO||YSZ and LNO||CGO cells can be attributed, most likely, to chemical reactivity between electrode and electrolyte materials in the course of the electrode fabrication, as supported by the results of XRD studies of powdered LNO+electrolyte mixtures calcined at 1050°C for 40h (Fig.5). The presence of non-negligible amount of pyrochlore-type $La_2Zr_2O_7$ phase was found for calcines LNO+YSZ mixture, together with traces of NiO. The segregation of insulating $La_2Zr_2O_7$ phase at the electrode/electrolyte interface is apparently responsible for the highest observed polarization resistance values (Table 2). Similarly, a second fluorite-type phase (in addition to NiO) was detected in XRD patterns of calcined LNO+CGO mixtures. The formation of this second fluorite phase is apparently promoted by reactivity between the LNO and CGO leading to a partial dissolution of lanthanum (originating from LNO) in ceria lattice. Even though $Ce(La)O_{2-\delta}$ is supposed to be a solid electrolyte with substantial ionic conductivity, the overall changes in the phase compositions at the LNO||CGO interface result in comparatively poor total kinetics of the electrode reaction and the R_p values only twice lower compared to LNO||YSZ. It is worth to mention here that similar reactions for other $La_{n+1}Ni_nO_{3n+1}$ phases in contact with YSZ (13,14) and CGO (14-16) solid electrolytes have been described and correlated with a poorer electrochemical performance. On the contrary, LNO appears to be less reactive in contact with LSGM, with only traces of $La_4Ni_3O_{10-\delta}$ and NiO phases detected at the background level in the XRD patterns of calcined LNO+LSGM mixture. RP-type $La_4Ni_3O_{10-\delta}$ itself is a good mixed conductor considered as a prospective electrode for SOCs devices (17-19) and apparently has a minimum impact on the performance of LNO||LSGM electrodes. On the other hand, one should be notice that a partial dissolution of LNO in the LSGM lattice cannot be excluded as noticeable variations in the intensity of some of the main diffraction peaks were observed after the calcination. Some works (20) show that minor NiO interdiffusion (≤5mol%) into LSGM due to interfacial reactivity at T ≤ 1350°C is acceptable and should not affect the oxygen-ionic conductivity of LSGM to significant extent. Furthermore, it was reported that

incorporation of moderate amounts (< 10 mol.%) of nickel into gallium sublattice of LSGM induces mixed conduction, with the values of ionic conductivity even higher compared to the parent LSGM (21), which can be expected to be favorable for the electrode performance. In any case, possible minor reactivity at the LNO||LSGM interface during the electrode fabrication has much smaller negative impact (if any) on the electrode performance if compared to other solid electrolytes.

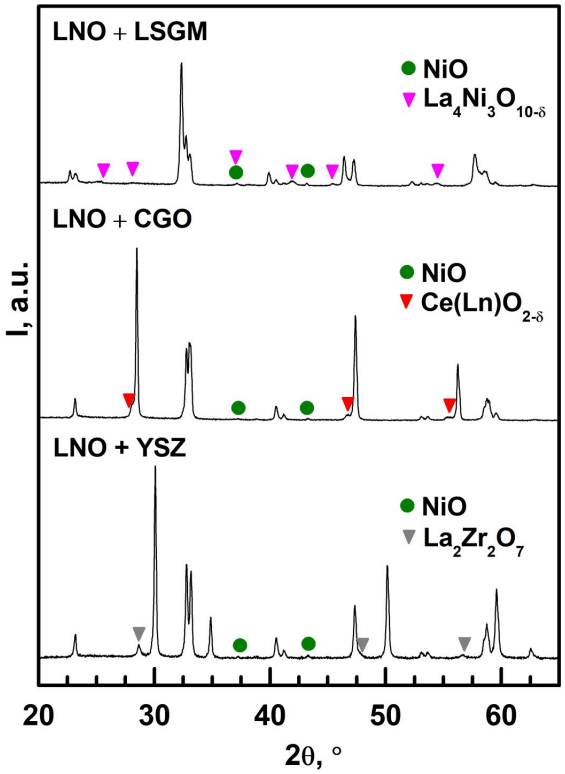

Figure 5. XRD patterns of powdered LNO+electrolyte mixtures after calcination in oxygen flow at 1050°C for 40 h.

The R_η values of LNO electrodes in contact with LSGM solid electrolyte can be further reduced by the surface modification with praseodymia down to 0.024 Ohm×cm^2 at 800°C and 0.11 Ohm×cm^2 at 700°C (LNO+PrO_x||LSGM cell in Table II). This improvement is probably related to the increase in catalytic activity since a significant decrease in the low-frequency contribution LF2 to the Nyquist plot was observed. At the same time, the activation energy of the electrode process remains unchanged after the surface modification with PrO_x. The enhancement of the electrocatalytic activity of the LNO+PrO_x electrodes may be related to the inherent mixed valence of Pr (4+/3+) species, which can expected to favor the oxygen evolution reaction (OER). A better understanding of the specific role of the PrO_x submicron particles in the OER at the SOC electrodes requires, however, further detailed electrochemical studies of praseodymia-containing oxygen electrodes.

The electrochemical performance of LNO-based electrodes in contact with LSGM was further assessed under steady-state anodic polarization by performing EIS studies of

3-electrode cells. The anodic overpotentials (η) of the LNO||LSGM cells under oxidizing conditions (≈ 76 and 114 mV at 800°C and 500 and 1000 mA×cm^{-2}, respectively) are comparable to those reported for some of the best SOEC oxygen electrode materials (4,5,22). Similar to the polarization resistance of symmetrical cells under zero-current conditions, the η values of LNO electrodes under anodic polarization were further decreased via surface modification with PrO_x. Fig.6 gives a representative example of the η values measured in air for the LNO+PrO_x||LSGM cell at 600-800°C. As depicted, the dependences of anodic overpotental on current density (*i*) are nearly linear under applied conditions. The measured η values at 800°C are as low as 20 and 39 mV at 500 and 1000 mA×cm^{-2}, respectively.

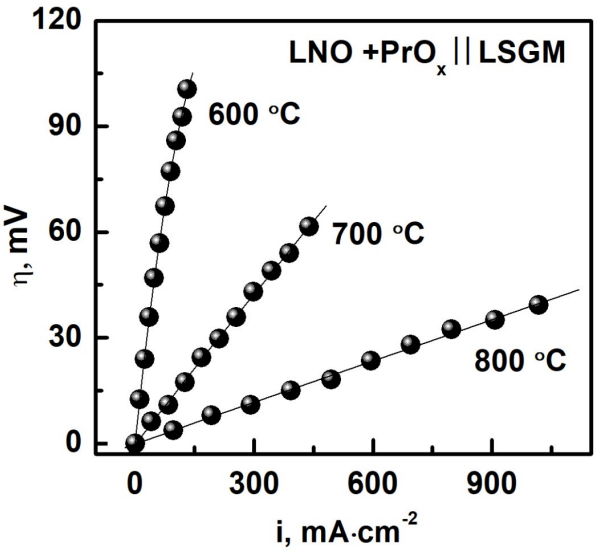

Figure 6. Dependence of anodic overpotential η of LNO+PrO_x||LSGM electrodes on current density at 600-800°C in air.

Thus, this work demonstrates a high electrochemical performance of LNO+PrO_x electrodes in contact with LSGM and highlights this type of composites as promising oxygen electrode materials for SOEC technology. The future planned work includes the assessment of a long-term performance of LNO-PrO_x electrodes and improvement of compatibility of these electrode materials with other solid electrolytes.

Conclusions

Within the phase stability domain, porous $LaNiO_{3-\delta}$ ceramics exhibit high *p*-type electrical conductivity and moderate thermal expansion coefficient compatible with common solid electrolytes. Polarization resistance of $LaNiO_{3-\delta}$ electrodes in contact with different solid oxide electrolytes decreases in the sequence YSZ < CGO < LSGM in correlation with the extent of chemical reactivity between electrode and electrolyte materials in the course of electrode fabrication. Surface modification of $LaNiO_{3-\delta}$ electrode with PrO_x submicron particles resulted in a noticeable reduction of the polarization resistance in contact with LSGM electrolyte down to to 0.024 Ohm×cm^2 at 800°C and 0.11 Ohm×cm^2 at 700°C under zero-current conditions in air. Steady-state

polarization studies of $LaNiO_{3-\delta}$+PrO_x electrodes in contact with LSGM demonstrated anodic overpotentials as low as 20 and 39 mV at 500 and 1000 $mA \times cm^{-2}$, respectively, at 800°C in air.

Acknowledgements

This work was done within the scope of project CARBOSTEAM (POCI-01-0145-FEDER-032295) and project CICECO - Aveiro Institute of Materials (FCT ref. UID/CTM/50011/2019), financed by national funds through the FCT/MCTES and when appropriate co-financed by FEDER under the PT2020 Partnership Agreement.

References

1. J. Kim, H.I. Ji, H.P. Dasari, D. Shin, H. Song, J.H. Lee, B.K. Kim, H.J. Je, H.W. Lee and K.J. Yoon, *Int. J. Hydrogen Energy*, **38**, 1225 (2013).
2. J.R. Mawdsley, J.D. Carter, A.J. Kropf, B. Yildiz and V.A. Maroni, *Int. J. Hydrogen Energy*, **34**, 4198 (2009).
3. D.O. Bannikov and V.A. Cherepanov, *J. Solid State Chem.*, **179**, 2721 (2006).
4. V.V. Kharton, E.V. Tsipis, A.A. Yaremchenko and J.R. Frade, *Solid State Ionics*, **166**, 327 (2004).
5. T. Ogier, F. Mauvy, J.M. Bassat, J. Laurencin, J. Mougin and J.C. Grenier, *Int. J. Hydrogen Energy*, **40**, 15885 (2015).
6. G. Amow and S.J. Skinner, *J. Solid State Electrochem.*, **10**, 538 (2006).
7. H.E. Höfer and R. Schmidberger, *J. Electrochem. Soc.*, **141**, 782 (1994).
8. T. Nakamura, G. Petzow and L.J. Gauckler, *Mater. Res. Bull.*, **14**, 649 (1979).
9. M. Zinkevich, N. Solak, H. Nitsche, M. Ahrens and F. Aldinger, *J. Alloy Compd.*, **438**, 92 (2007).
10. V. Dusastre and J.A. Kilner, *Solid State Ionics*, **126**, 163 (1999).
11. J.C. Ruiz-Morales, D. Marrero-López, J.T. Irvine and P. Núñez, *Mater. Res. Bull.*, **39**, 1299 (2004).
12. F. Mauvy, C. Lalanne, J.M. Bassat, J.C. Grenier, H. Zhao, L. Huo and P. Stevens, *J. Electrochem. Soc.*, **153**, A1547 (2006).
13. H. Zhao, F. Mauvy, C. Lalanne, J.M. Bassat, S. Fourcade and J.C. Grenier, *Solid State Ionics*, **179**, 2000 (2008).
14. A.M. Hernández, L. Mogni and A. Caneiro, *Int. J. Hydrogen Energy*, **35**, 6031 (2010).
15. A. Montenegro-Hernandez, J. Vega-Castillo, L. Mogni, A. Caneiro, *Int. J. Hydrogen Energy*, **36**, 15704 (2011).
16. R. Sayers, J. Liu, B. Rustumji and S.J. Skinner, *Fuel Cells*, **8**, 338 (2008).
17. R.J. Woolley and S.J. Skinner, *Solid State Ionics*, **255**, 1 (2014).
18. R.J. Woolley and S.J. Skinner, *J. Power Sources*, **243**, 790 (2013).
19. R.K. Sharma, M. Burriel and E. Djurado, *J. Mater. Chem. A*, **3**, 23833 (2015).
20. P. Huang, A. Horky and A. Petric, *J. Am. Ceram. Soc.*, **82**, 2402 (1999).
21. T. Ishihara, T. Shibayama, H. Nishiguchi and Y. Takita, *J. Mater. Sci.*, **36**, 1125 (2001).
22. B. Wei, J. Feng, L. Zhu, Z. Wang, X. Zhu, X. Huang, Y. Zhang, L. Xu, H. Gao and Z. Lü, *J. Eur. Ceram. Soc.*, **38**, 2396 (2018).